https://doi.org/10.46861/bmp.29.255 PŮVODNÍ PRÁCE/ORIGINAL PAPER

Mineralogy of the Au-Ag mineralization from the Finsterort and Anton vein system, Štiavnické vrchy Mts. (Slovakia)

Jozef Vlasáč[1)], Martin Chovan[2)], Rastislav Vojtko[3)], Peter Žitňan[3,4)] and Tomáš Mikuš[1)]*

[1)]*Earth Science Institute, Slovak Academy of Sciences, Ďumbierska 1, 974 01 Banská Bystrica, Slovakia; *e-mail: mikus@savbb.sk*
[2)]*Department of Mineralogy, Petrology and Economic Geology, Faculty of Natural Sciences, Comenius University in Bratislava, Ilkovičova 6, 842 15 Bratislava, Slovakia*
[3)]*Department of Geology and Palaeontology, Faculty of Natural Sciences, Comenius University in Bratislava, Ilkovičova 6, 842 15 Bratislava, Slovakia*
[4)]*Rudné Bane š.p., Kammerhofská 25, 969 01 Banská Štiavnica, Slovakia*

Vlasáč J, Chovan M, Vojtko R, Žitňan P, Mikuš T (2021) Mineralogy of the Au-Ag mineralization from the Finsterort and Anton vein system, Štiavnické vrchy Mts. (Slovakia). Bull Mineral Petrolog 29(2): 255-269 ISSN 2570-7337

Abstract

The Finsterort and Anton vein system is located in the central zone of the Middle Miocene Štiavnica Stratovolcano between Vyhne and Hodruša-Hámre villages. The vein system contains several partial veins and veinlets and has generally NNE - SSW strike with moderate to steep eastward dip. Kinematics of the veins is characterised by older dextral strike-slip movement replaced by younger normal faulting. The mineralization is associated with the normal faults and the veins contain interesting paragenesis of Au-Ag bearing minerals. Minerals of precious metals are represented by argentotetrahedrite-(Zn) and rozhdestvenskayaite-(Zn), Au-Ag alloys, members of polybasite-pearceite and pyrargyrite-proustite solid solutions, acanthite and uytenbogaardtite. Au-Ag mineralization is accompanied by older paragenesis comprising mainly pyrite, galena, sphalerite and chalcopyrite. Besides quartz, carbonates (calcite, siderite and dolomite) are the main gangue minerals.

Key words: *Western Carpathians, Neogene Štiavnica Stratovolcano, normal faults, Ag bearing phases, rozhdestvenskayaite-(Zn)*

Received 11. 10. 2021; accepted 6. 12. 2021

Introduction

The Central Slovakia Volcanic Field hosts several famous Ag-Au epithermal vein-type deposits including Banská Štiavnica, Kremnica, Hodruša-Hámre, Nová Baňa, and Pukanec, which were important sources of precious and base metals in the past. Mineralogical research from those deposits yielded a lot of interesting results in the last decades in respect to the Au and Ag-bearing phases (Majzlan 2009; Berkh et al. 2014; Majzlan et al. 2016; Kubač et al. 2018; Majzlan et al. 2018; Števko et al. 2018 and Chovan et al. 2019). The history of mining on Anton -Finsterort vein system dates back to 14th century (Kaňa 2016). Mining activities have been carried out continuously since the late 19th century. The mining and processing of Au-Ag ores in Hodruša - Vyhne area finally deceased in 1950 (Bakos ed. 2017). The richer upper parts of the Finsterort - Anton vein system were mined a long time ago, that's why modern mineral identification wasn't done yet. The occurrence of Ag sulphides in quartz and carbonate veins is mentioned in mineralogical monographs of the Western Carpathians (Koděra ed. 1986; Ďuďa, Ozdín 2012). Onačila, Rojkovičová (1992) reported electrum, freibergite, pyrargyrite, polybasite, stephanite, miargyrite and acanthite from the Hodruša veins. White-yellow quartz, amethyst, dolomite, manganocalcite, and baryte were described from the Finsterort and Anton veins. Polybasite and stephanite are the most common among ore minerals. Acanthite, pyrargyrite and rarer proustite, pearceite, and Ag tetrahedrite-freibergite are also abundant. Sphalerite is most common among base-metal sulphides. Galena, chalcopyrite and pyrite are rare (Koděra ed. 1986; Ďuďa, Ozdín 2012).

The main goal of this paper is to characterise Au-Ag minerals in selected veins of the Hodruša-Vyhne area. The next aim is to describe geometrical characteristics and kinematics of faults related to vein system and tectonic evolution of the Au-Ag mineralisation in the central zone of Štiavnica Stratovolcano in the Finsterort and Anton vein system.

Geological settings

Ore veins in Hodruša-Hámre and Vyhne are located in the central zone of a large Middle Miocene Štiavnica Stratovolcano, which belongs to the western part of the Central Slovakia volcanic field (Fig. 1). It represents the largest volcano of the volcanic field covering almost 2500 km^2 area. The characteristic features of the mainly andesite stratovolcano include an extensive caldera (approx. 20 km in diameter), a late stage resurgent horst in the caldera centre and an extensive subvolcanic intrusive complex (Konečný et al. 1995). The volcanic activity is dated to Middle and Late Miocene (~ 16.5 - 8.5 Ma) and comprises mainly of various types of Badenian and Sarmathian andesites with minor proportions of Sarmatian to Pannonian rhyolites and sporadic Pannonian to Quaternary basalts. Pre-volcanic basement consists of Veporic

granodiorite and its sedimentary cover and Silicic and Hronic nappes (limestones, dolomites and quartzites). Most of the Miocene volcanic rocks are chemically similar to medium to high-K andesites of continental margins or evolved island arcs involving older continental crust (Konečný et al. 1995). The intrusive rocks represent diorites, granodiorites to monzonites and smaller intrusion bodies of granodiorite, quartz-diorite and andesite porphyries (Lexa et al. 1999a). Petrographic and geochemical investigations suggested a mantle source of the primary basaltic magma with variable crustal contamination and differentiation in a shallow magma chamber (Konečný et al. 2002; Rottier et al. 2020). Late-stage rhyolites indicate melting of crustal material over a shallow magma chamber and magma mixing. Neogene volcanism was related closely in space and time to back-arc extensional processes, giving rise to horsts and grabens. These processes eventually formed beneficial conditions that led to the evolution of a long-lasting hydrothermal system and formation of various mineralization types, ranging from intrusion-related magnetite skarn, base-metal stockwork, and metasomatic base metal to epithermal Au-Ag-base metal mineralization (Lexa et al. 1999a). The ore mineralization occurs within or around the subvolcanic intrusive complexes (Kovalenker et al. 2006). The associated hydrothermal activity formed an extensive epithermal system including 120 veins and veinlets predominantly of NE - SW strike, covering almost 100 km^2 (Lexa et al. 1999a). Based on structural aspects, vertical extent, spatial distribution and dominant mineral paragenesis, three types of epithermal veins were distinguished (Lexa et al. 1999a, b; Lexa 2001): 1) sulphide-rich base-metal veins ± Au, in the east-central part of the horst ("Štiavnica type"); 2) Ag-Au ± base-metal veins in the central-western part of the horst ("Hodruša type"); and 3) Au-Ag veins related to marginal faults of the horst ("Kremnica type"). The "Štiavnica type" veins are vertical by zoned with Au-Ag, upper and lower Pb-Zn, and Cu zones (Koděra 1963).

Anton-Finsterort (Alžbeta) veins are typical low-sulphidation Ag-Au veins of the Hodruša type linked to the development of the horst-graben structures in Štiavnica volcano (Lexa et al. 1999a). The vein structure is probably one and the same structure in structural terms, albeit it has several names - Alžbeta, Brenner and Finsterort in southern part in Hodruša and Anton vein in northern part in Vyhne. Anton vein is hosted mainly in the Veporic granodiorite and its sedimentary cover rocks (limestones, quartzites), less in Miocene andesites and quartz-diorite porphyries. Alžbeta and Finsterort veins are hosted in strongly altered Miocene andesites, granodiorite and quartz-diorite porphyries.

Sampling and analytical methods

The studied ore samples were collected at the waste dump of the Brenner - sv. Trojice adit (Finsterort vein structure) in Hodruša-Hámre village and from the same vein structure - Anton vein from the waste dumps of Anton adit in the Vyhne area. Polished and thin sections were prepared for microscopic study in reflected light. Electron microprobe analyses (EMPA) of sulphides and

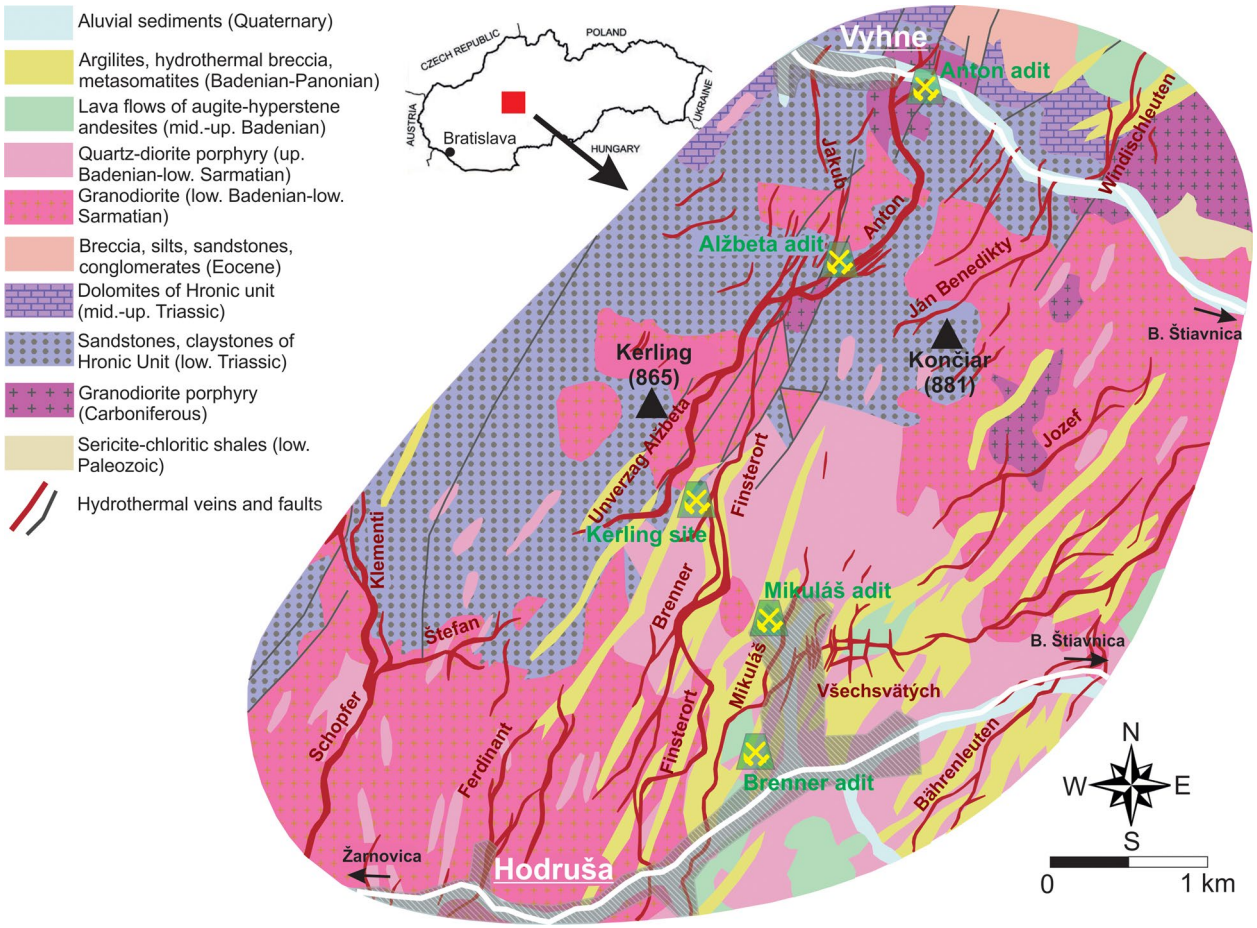

Fig. 1 *Simplified geological map of the Hodruša-Hámre - Vyhne area after Konečný et al. (1998) with location of main ore structures.*

carbonates were performed on a JEOL JXA 8530FE in a wavelength-dispersive mode (WDS) at the Earth Sciences Institute of Slovak Academy of Sciences in Banská Bystrica under the following conditions for carbonates: accelerating voltage 15 kV, probe current 16 nA, beam diameter 10 μm. Peak counting times were 10 - 20 s, and one-half of the peak time was used for each background. Raw intensities were converted to the concentrations of elements using automatic ZAF matrix-correction software. Following X-ray lines and standards were used: Ca(*K*α) and Mg(*K*α) - diopside, Si(*K*α) - quartz, K(*K*α) - orthoclase, Al(*K*α) - albite, Mn(*K*α) - rhodonite, Fe(*K*α) - hematite, Sr(*L*α) - celestite, Ba(*L*α) - baryte. For sulphides, sulphosalts and Au alloys were used following condition: accelerating voltage 20 kV, probe current 15 nA, beam diameter 5 - 10 μm. Peak counting times were 20 s, and one-half of the peak time was used for each background. Raw intensities were converted to the concentrations of elements using automatic ZAF matrix-correction software. Following X-ray lines and standards were used: S(*K*α) - pyrite, Sb(*L*α) - stibnite, Ag(*L*α) - Ag, Au(*M*α) - Au, Te(*L*α) - CdTe, As(*L*β) - GaAs, Se(*L*α) - Bi_2Se_3, Bi(*L*α) - Bi_2S_3, Cu(*K*α) - chalcopyrite, Fe(*K*α) - pyrite, Pb(*M*α) - galena, Hg(*M*β) - cinnabar.

Structural analysis was focused on characterisation of the geometry, kinematics and structural evolution of veins. The geometry and attitude of veins was determined by standard procedures of structural geology using geological compass. Obtained data were processed by the stereographic projection techniques. Kinematic analysis on faults related to vein formation was carried out mainly on fault surfaces with slickensided lineations (striae) as an indicator of movement on a fault plane. Faults and striae on the fault surfaces are very often present in rocks and therefore kinematic and dynamic analysis of fault-slip data is very popular tool for reconstruction of palaeostress fields.

Standard procedures for brittle fault-slip analysis and palaeostress reconstruction are now well established (Angelier 1990, 1994; Etchecopar et al. 1981; Michael 1984). The obtained data were registered and line-plane pairs validated using the GeolCalc software (R. Vojtko). After the initial processing, these data were used for spatial, fault-slip analysis and palaeostress reconstruction by TectonicsFP (http://www.tectonicsfp.com; by F. Reiter and P. Acs) software using the P-T-axes method. P- B- and T-axes are calculated with the selected theta angle for each fault plane after Turner (1953). For the calculation, bivalent datasets are treated as reverse faults. P- and T-axes are exchangeable for these data. TectonicsFP shows theta angles and R% of P- and T-axes for maximum clustering (= maximal R%) of P-, T- and for both P- and T axes (R(p) multiplied by R(t)).

Visualisation of analysed data was performed by TectonicsFP (Angelier plot) and contour plots of P- and T-axes was calculated by StaTect software (http://www.eltekto.cz; J. Rez). The contoured plots were calculated using either the 1% circle. The smoothing parameter was set with maxima 64, which gave the sharpness comparable to the 1% circle method). The 1% circle method gave values in percent.

Mineral symbols used in figures are adopted after Warr (2021).

Results

Structure

The precious metal Finsterort and Anton veins are located between the villages of Vyhne to the north and Hodruša-Hámre to the south in the central zone of the Štiavnica Stratovolcano. Generally, the veins have NNE - SSW strike with moderate to steep dip to the ESE with a distinct flexure in the southern part of Anton vein (Fig. 1). The Anton vein in its northern end changes the dip direction from 60 - 70° ESE through the vertical to approx. 70° WSW and has helicoidal geometry of an individual Riedel shear. The Anton vein system is located in the northern part, while the Finsterort veins are located in the southern part of the study area. The geometry and kinematics of the vein system was investigated in abandoned mining works (Alžbeta adit, Mikuláš adit, and Kerling mining works; for the position see Fig. 1). These sites are well distributed and are representing all parts of the vein system (north, middle and south section).

The Alžbeta adit

The structural measurements were carried out in the Alžbeta adit - in the northern part of the Anton vein system. Based on the structural analysis, four homogeneous structures were distinguished.

The oldest homogeneous set of structural data is related to low angle normal fault-slips dipping to the north with the extensional tectonic regime with generally N - S trending extensional axis σ_3 (Fig. 2a).

The second monogenetic group is represented by conjugate steeply dipping W - E striking normal faults originated during the extensional tectonic regime with generally N - S trending extensional axis σ_3 (Fig. 2b). The second group of faults is older than the Anton vein (fault) and younger than the low angle normal faults of the first group.

The third and fourth homogeneous fault-slip groups, whose stereograms are shown on Fig. 2c, d, are linked with the evolution of the Anton vein (fault). However, the evolution of the Anton vein started as a dextral strike slip fault, which is not presented in stereograms because only one fault-slip was observed and measured. The strike of the fault plane is NE - SW with dipping SE-wards and striae almost subhorizontal.

The strike-slip slickensided lineations are overprinted by the normal faulting of the third group of faults. The Anton vein was opened during the pure normal faulting with the fault strike NNE - SSW to NE - SW and inclination of fault (vein) planes SE-wards and are related to extensional tectonic regime with the NW - SE-trending extensional axis (Fig. 2c).

The younger movement on the fault planes of the Anton vein structure is linked to extensional tectonic regime with the W - E-trending extensional axis σ_3. The kinematics of faults changed to oblique normal faults with sinistral component (Fig. 2d).

The Kerling site

The Kerling historical mining workings are located in the middle part of the Anton - Finsterort vein system. The site consists of surface and underground mining works with well uncovered thick vein, which was subject to historical production. Based on the structural analysis, two distinctive homogeneous fault-slips groups were distinguished (Fig. 3). The strike of the measured fault planes is

in both groups the same in NE - SW direction and moderately inclined SE-wards. However, the slickensided lineations have different trend. The first group of fault-slips is defined by SE trending slickensided lineations, which refer to the pure normal faults practically with no horizontal movement component. The fault-slip data of the main vein structure originated under condition of extensional tectonic regime with the NW - SE-trending σ_3 axis (Fig. 3a).

The movement on the main fault zone (vein) was later replaced from the normal fault to oblique slip normal fault kinematics of the second homogeneous group of fault-slips. The slickensided lineations on fault planes have ENE -trend and these younger fault-slip data of the main vein structure are related to extensional tectonic regime with the ~ W - E-trending σ_3 axis.

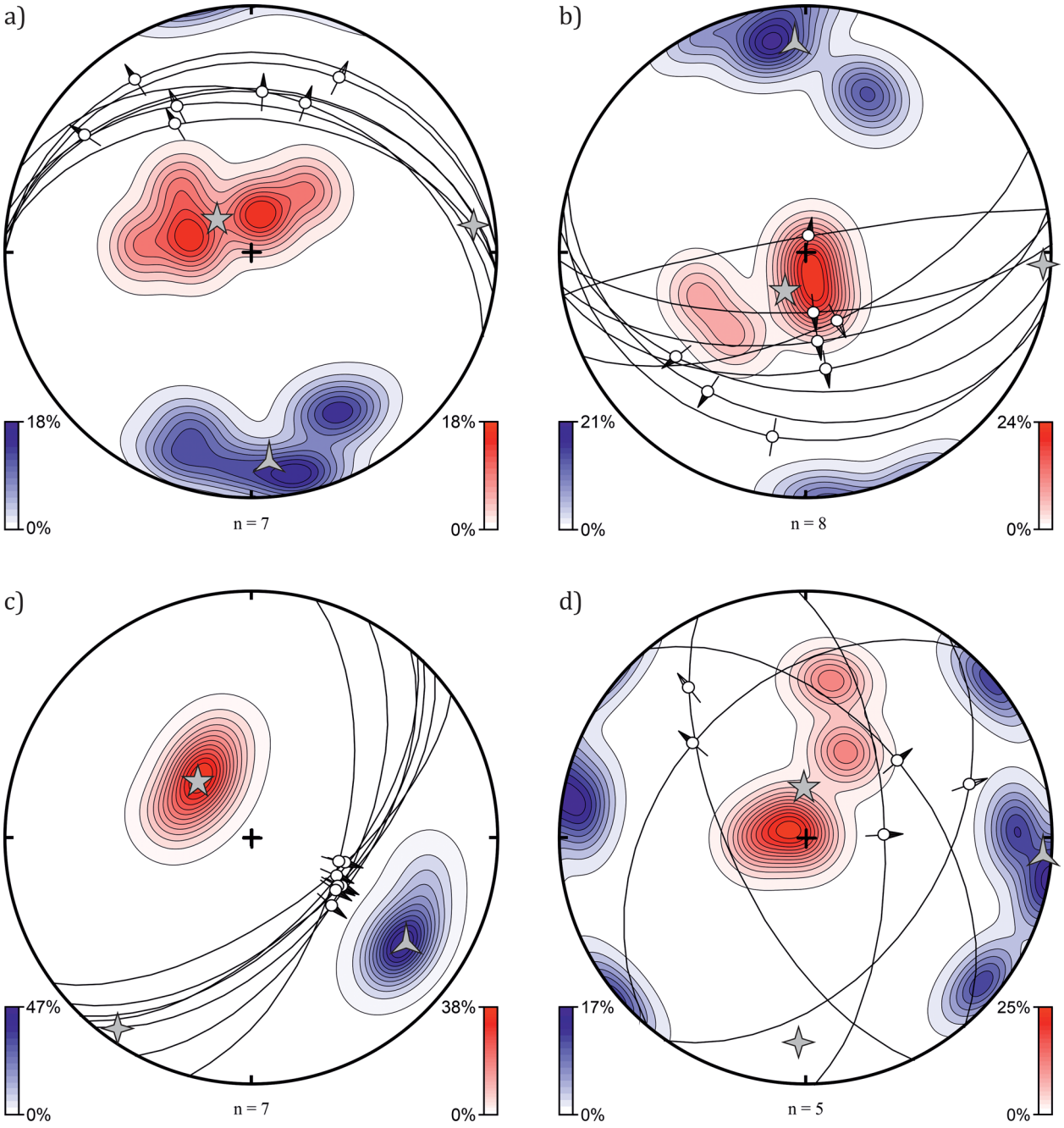

Fig. 2 *Stereograms of mineralised structures in the Alžbeta adit (Anton vein): a) low angle normal fault-slips with extensional tectonic regime with generally N - S trending extensional axis: P 315/74° (89% probability), B 083/10° (80%), and T 175/18° (89%); b) conjugate steeply dipping normal faults, which are older than Anton vein (fault) originated during the extensional tectonic regime with generally N - S trending extensional axis: P 209/76° (91%), B 092/04° (87%), and T 357/16° (89%); c) older fault-slip data of the Anton vein structure related to extensional tectonic regime with the NW - SE-trending extensional axis: P 317/64° (98%), B 215/06° (96%), and T 123/26° (98%); d) younger fault-slip data of the Anton vein structure related to extensional tectonic regime with the W - E-trending extensional axis: P 358/73° (84%), B 182/18° (67%), and T 093/04° (78%).*

The Mikuláš adit

The Mikuláš adit is situated in the SE portion of the subject vein system (Alžbeta, Brenner and Finsterort) practically in the historical center of Banská Hodruša settlement. The structural measurements were carried out inside the adit in the main corridor and mining works driving along the vein. The measured structures are polygenetic and belong to three homogeneous fault-slip groups. The older faulting preceding the formation of main vein system is characterised by NE - SW strike with the very gently dipping reverse fault NW-wards and gently dipping normal fault SE-wards. These low-angle fault-slips, predominantly reverse faults, were affected by tilting caused by normal faulting on the Finsterort-Anton vein system (Fig. 4a). However, formerly low-angle reverse fault-slips have to be rotated to original position along the rotational axis *R* 020/01° with the angle 25°. After the tilt rotation, the fault-slips get in original position when they were formed (Fig. 4b). This is in line of other evidences in the broader area of the Mikuláš adit (cf. Kubač et al. 2018; Vojtko et al. 2019) and these low angle normal faults originated during the extensional tectonic regime with the WNW - ESE trending σ_3 axis.

The main vein system is related to NE - SW striking normal faults with moderate SE-ward inclinations which significantly disrupt the aforementioned low angle faults. The fault system was activated by extensional tectonic regime with the WNW - ESE trending σ_3 axis (Fig. 4c), which represents older homogeneous group of fault-slip data linked to the main vein. The younger fault-slips observed in the main vein structure are related to extensional tectonic regime with the W - E-trending extensional axis. It should be noted that a NE - SW strike-slip on main fault plane (vein) was also observed in this case and is considered to be older than dip-slip faults associated with normal faulting.

Mineralogy

Macroscopically, the ore shows hydrothermal breccia textures and symmetrical banded textures. The ore minerals are finely scattered in a quartz-carbonate vein and are arranged in stripes and edges around fragments of altered rock (Fig. 5). Tabular crystals of baryte up to 2 cm and fragments of amethyst druses (several cm) were also found on the waste dumps.

Ag-bearing phases and gold are accompanied by base-metal sulphides which belong to older mineral assemblage. *Pyrite* is one of the most common sulphides. It is disseminated in strongly altered host rock, or forms anhedral, subhedral grains or aggregates up to 400 μm. Pyrite aggregates are often replaced by Fe-oxyhydroxides. Rarely, pyrite is cataclased and fissures are filled by Fe-oxyhydroxides. Pyrite is often associated with *galena* and *sphalerite*. They form aggregates up to several mm in size. *Chalcopyrite* occurs only rarely. All phases from this stage are intensively replaced by younger Ag-sulphosalts.

Au-Ag minerals

Gold (Au-Ag alloy) was identified in both occurrences and it is quite rare. It forms irregular grains up to 20 μm in size. Gold typically shows strong irregular chemical zoning in back-scatter electron images (BSE). Gold grains are often rimmed with younger, higher fineness gold rims (Fig. 6a). The rims could represent the younger generation of gold, or it could be a result of supergene? remobilisation and gold-enrichment. Gold is frequently associated with Ag minerals (pyrargyrite, proustite, pearceite and acanthite) and galena. Highly variable Ag content is shown in Figure 7. The silver content in rims reaches up to 16.54 wt. % (0.26 *apfu*). The silver content in the heterogeneous gold grains ranges from 37.16 to 49.07 wt. % (0.52 - 0.64 *apfu*). Contents of Hg, Te, Cu and Fe in gold are negligible. Selected microprobe analyses of gold are given in Table 1.

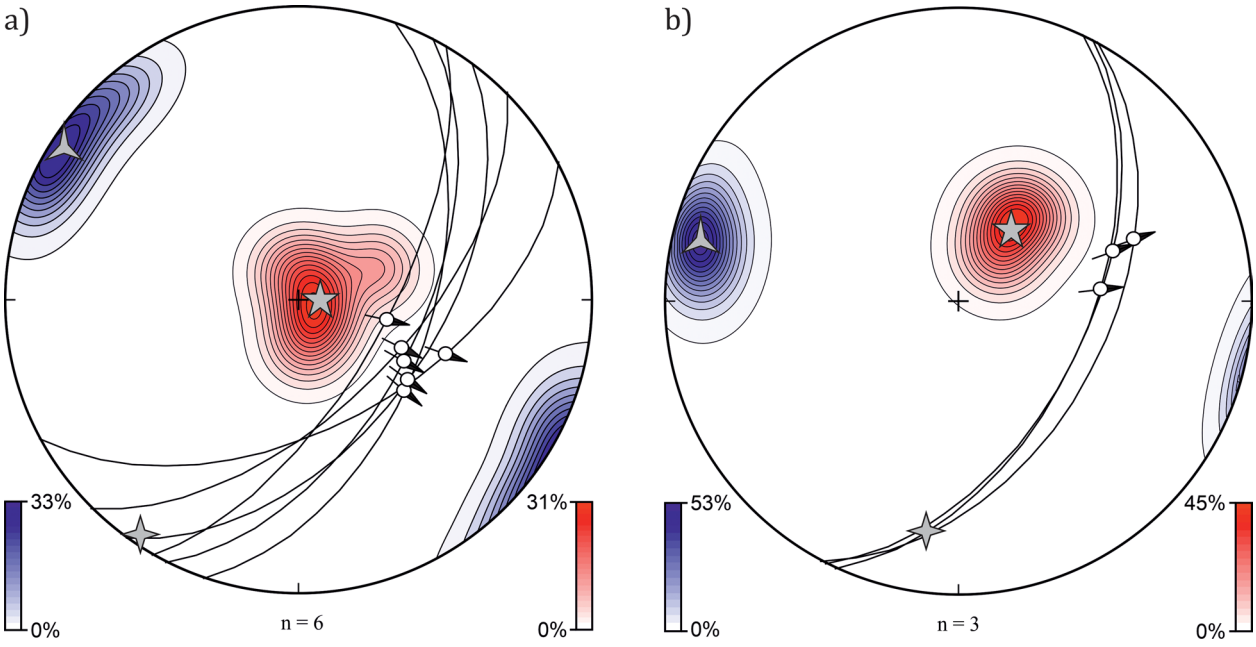

Fig. 3 *Stereograms of mineralised structures in the Kerling abandoned mining works (mean vectors): a) older fault-slip data of the main vein structure related to extensional tectonic regime with the NW - SE-trending σ_3: P 086/84° (96%), B 214/04° (95%), and T 304/04 (97%); b) younger fault-slip data of the main vein structure providing extensional tectonic regime with the ~ W - E-trending σ_3: P 036/65° (99% probability), B 188/22° (99%), and T 283/11° (99%).*

Uytenbogaardtite Ag_3AuS_2 is another Au bearing phase at both occurrences. It was found rarely as anhedral grains up to 10 μm in size associated with acanthite as the youngest sulphidic phase. The chemical composition of uytenbogaardtite is slightly different from the theoretical composition, namely by lower Au contents (Tab. 2). This difference is probably caused by its instability under the electron beam or by its porous character.

Ag sulphides

Acanthite Ag_2S is the most common silver sulphide in both occurrences, which is almost always associated with other Ag-Au bearing phases. Two generations of acanthite were identified in studied samples. The first generation occurs as compact, massive grains up to 200 μm in size, associated with polybasite-pearceite (Fig. 8a, c), pyrargyrite-proustite and gold. All associated Ag-Au phases are often replaced by acanthite. The second generation forms porous anhedral grains up to 20 μm in size or thin porous rims around Ag-sulphosalts. The porous grains are

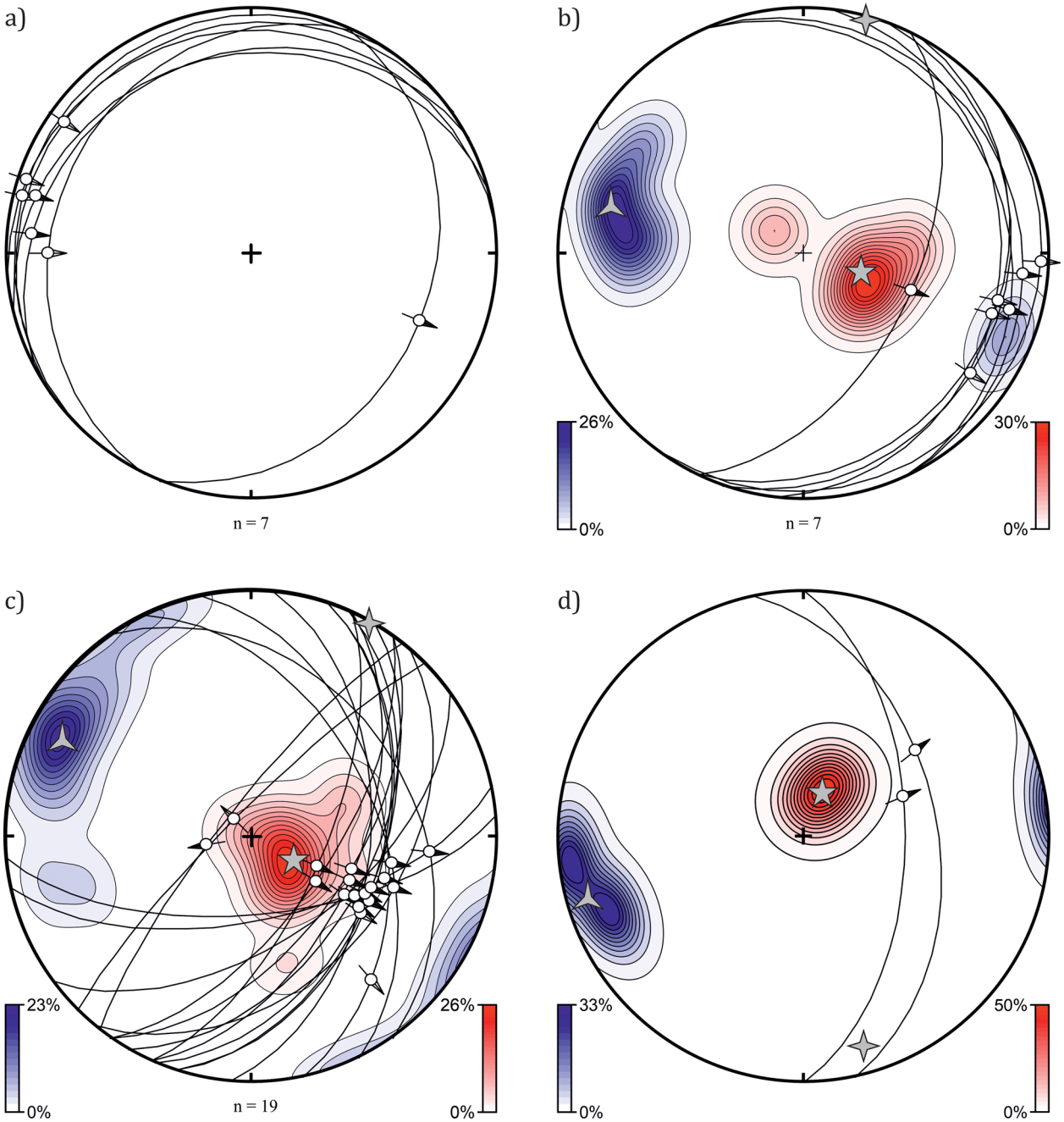

Fig. 4 *Stereograms of mineralised structures in the Mikuláš adit (Mikuláš vein): a) low-angle fault-slips, predominantly reverse faults affected by tilting; b) formerly low-angle reverse fault-slips, rotated to original position with the normal faulting along the rotational axis R 020/01° with the angle 25°: P 107/70° (93%), B 015/02° (96%), and T 285/20° (92%); c) older fault-slip data of the main vein structure related to extensional tectonic regime with the NW - SE -trending extensional axis: P 118/74° (93%), B 029/01° (84%), and T 298/14 (87%); d) younger fault-slip data of the main vein structure related to extensional tectonic regime with the W - E-trending extensional axis P 023/74° (99%), B 164/12° (99%), and T 255/10° (99%).*

associated with uytenbogaardtite and rozhdestvenskayaite-(Zn). Due to strong porosity, some analyses may be subject to analytical error, thus stoichiometry may not be chemically correct. WDS analyses showed the minor presence of some other elements like Cu and Te (Tab. 3).

Ag-Sb(-As) sulphosalts

Minerals of **pyrargyrite-proustite series Ag_3SbS_3-Ag_3AsS_3** are one of the most common sulphosalts at the examined localities. They occur as euhedral to anhedral grains and aggregates up to 150 μm in size and are associated with polybasite-pearceite, acanthite and gold. They are very often heterogeneous and show very strong sector (Fig. 6a) or oscillatory zoning (Fig. 6c) in BSE. The chemical composition of the identified pyrargyrite and proustite (Fig. 9) concentrate around endmember compositions mainly, nevertheless the almost complete range of solid solution between pyrargyrite and proustite was documented. Studied minerals of the proustite-pyrargyrite series are characterised by the wide range of Sb/(Sb + As) ratio ranging from 0.01 to 0.27 in proustite and 0.57 to 0.99 in pyrargyrite respectively (Tab. 4, 5).

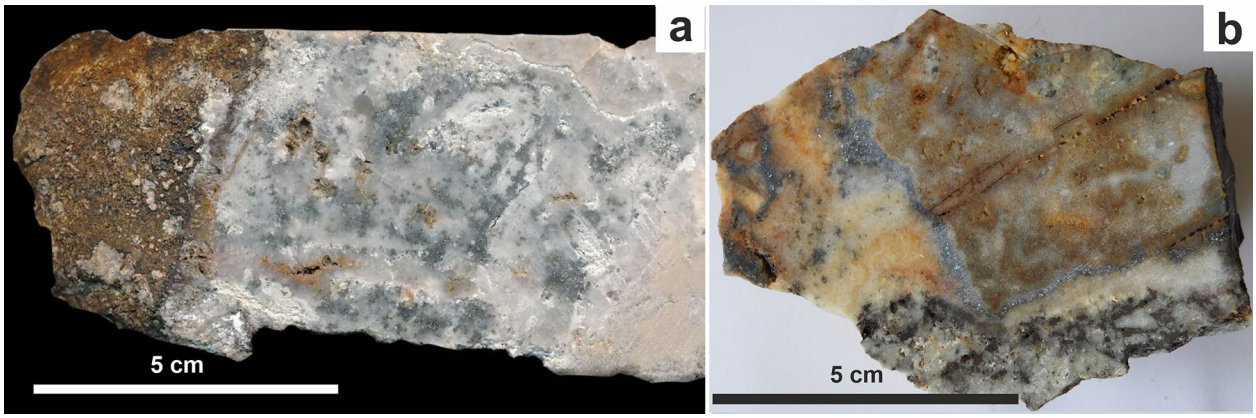

Fig. 5 *Examples of studied ore textures: a) Vyhne - Anton vein; b) Hodruša - Finsterort vein.*

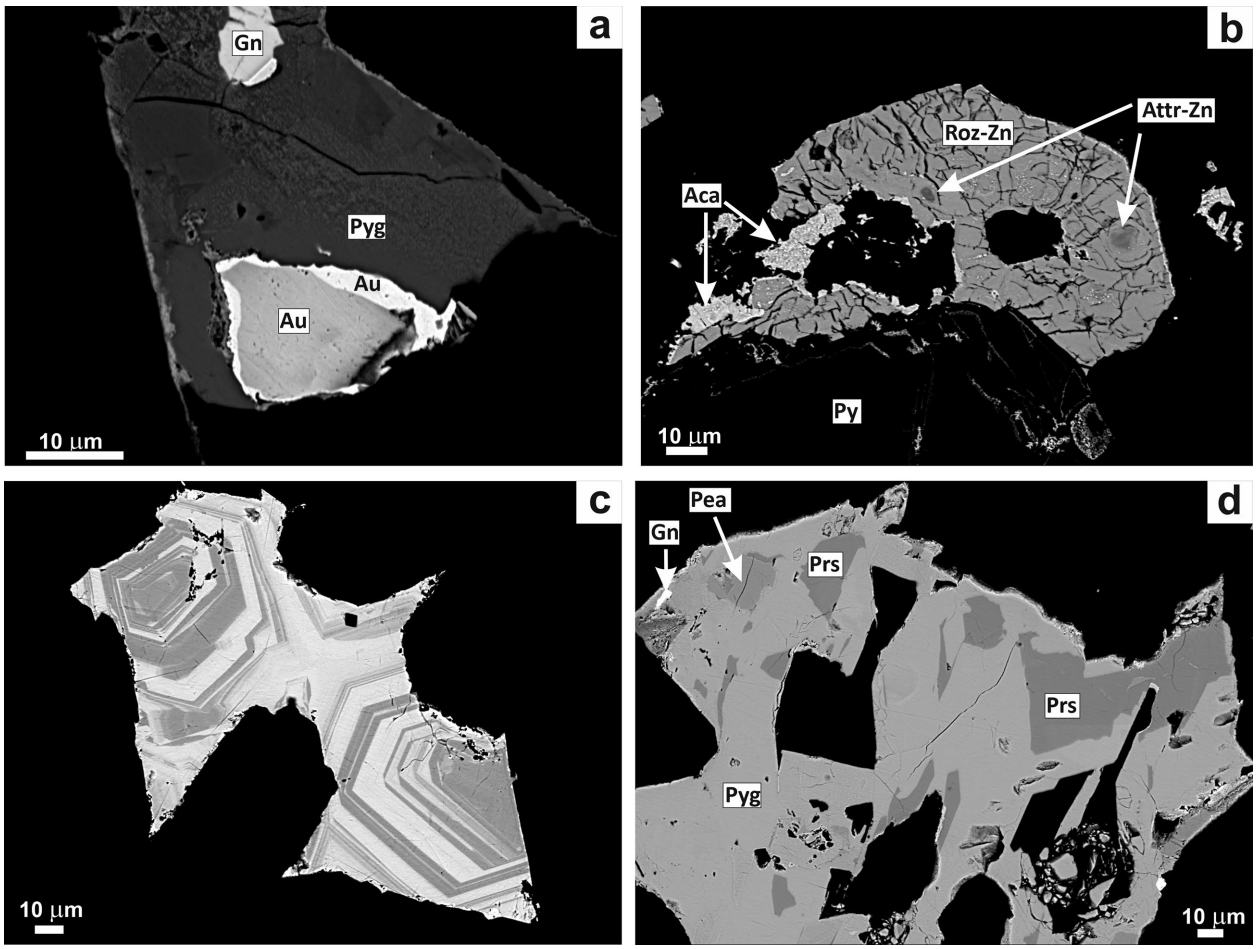

Fig. 6*a* *- Gold (Au) particle associated with heterogeneous pyrargyrite (Pyg) and galena (Gn).* ***b*** *- Aggregate of rozhdestvenskayaite-(Zn) (Roz-Zn) is replacing argentotetrahedrite-(Zn) (Attr-Zn) and is intensively replaced by porous acanthite (Aca).* ***c*** *- Extremely zoned pyrargyrite-proustite grain in the quartz vug.* ***d*** *- Aggregate of silver minerals consisting of pyrargyrite (Pyg), proustite (Prs) and pearceite (Pea) accompanied by galena (Gn). All samples are from the Finsterort vein. All images are back-scattered images from microprobe.*

Table 1 *Chemical composition of Au-Ag alloys from the Finsterort (F) and Anton (A) vein. Thin Au rims were not analysed*

	F-1	F-2	F-3	F-4	F-5	F-6	A-1	A-2	A-3	A-4
Ag	49.07	47.42	42.85	39.57	37.16	16.55	53.36	48.89	44.62	44.18
Fe	0.08	0.04	0.04	0.03	0.00	0.00	0.04	0.03	0.71	0.00
Cu	0.00	0.00	0.08	0.00	0.00	0.02	0.01	0.00	0.18	0.00
Te	0.10	0.16	0.07	0.54	0.07	0.12	0.14	0.13	0.61	0.57
Au	49.81	51.92	56.52	59.43	62.52	83.70	46.73	49.22	53.75	55.25
Bi	0.03	0.00	0.00	0.11	0.05	0.32	0.01	0.11	0.09	0.10
S	0.12	0.16	0.05	0.12	0.10	0.09	0.12	0.15	0.00	0.18
Hg	0.09	0.05	0.07	0.07	0.03	0.03	0.02	0.20	0.01	0.16
∑(wt%)	99.30	99.76	99.67	99.87	99.93	100.82	100.43	98.72	99.98	100.44
Ag	0.637	0.619	0.577	0.541	0.517	0.263	0.671	0.638	0.585	0.584
Fe	0.002	0.001	0.001	0.001	0.000	0.000	0.001	0.001	0.018	0.000
Cu	0.000	0.000	0.002	0.000	0.000	0.000	0.000	0.000	0.004	0.000
Te	0.001	0.002	0.001	0.006	0.001	0.002	0.002	0.001	0.007	0.006
Au	0.354	0.371	0.417	0.445	0.477	0.727	0.322	0.352	0.386	0.400
Bi	0.000	0.000	0.000	0.001	0.000	0.003	0.000	0.001	0.001	0.001
S	0.005	0.007	0.002	0.006	0.005	0.005	0.005	0.006	0.000	0.008
Hg	0.001	0.000	0.000	0.000	0.000	0.000	0.000	0.001	0.000	0.001

Analyses are recalculated on the basis of 1 *apfu*

Table 2 *Chemical composition of uytenbogaardtite from the Finsterort (F) and Anton (A) vein*

	F-1	F-2	F-3	F-4	A-1	A-2
Ag	55.74	53.75	53.38	55.01	55.68	56.57
Te	0.48	0.54	0.10	0.58	0.08	0.56
Cu	0.53	0.53	0.33	0.55	0.07	0.12
S	11.75	12.28	11.25	11.18	10.93	10.54
Au	32.23	33.25	33.47	32.94	32.71	32.56
∑(wt%)	100.72	100.35	98.53	100.25	99.48	100.35
Ag	2.928	2.813	2.906	2.945	3.021	3.071
Te	0.021	0.024	0.005	0.026	0.004	0.026
Cu	0.047	0.047	0.031	0.050	0.007	0.011
S	2.077	2.162	2.060	2.014	1.996	1.925
Au	0.927	0.953	0.998	0.966	0.972	0.968

Analyses are recalculated on the basis of 6 *apfu*

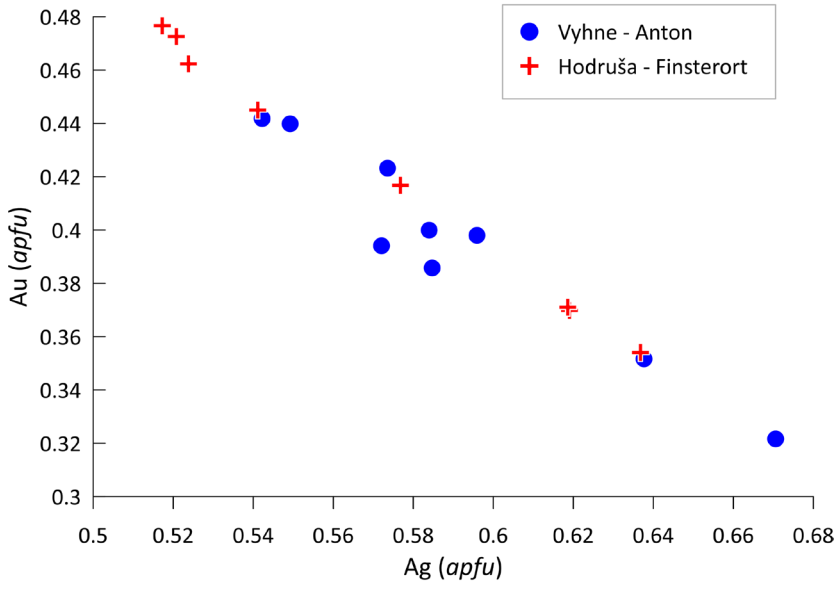

Fig. 7 *Graph of Ag vs. Au (apfu) for of Au-Ag alloy from the studied localities.*

Ag-Cu sulphosalts

Minerals of the **polybasite group** **$[Ag_9CuS_4][(Ag,Cu)_6(As,Sb)_2S_7]$** are very common at both occurrences. They form euhedral to anhedral grains up to 150 μm size, usually accompanied by pyrargyrite, proustite, acanthite, gold, galena and minerals of the tetrahedrite group. Minerals of this solid solution series often show strong chemical zoning in BSE (Fig. 8b). Chemically, the two members of the polybasite group were determined in the studied material: polybasite and pearceite with high extent of Ag-Cu and Sb-As substitutions (Fig. 10). Cu content in **polybasite** ranges in the interval 1.35 - 2.68 *apfu* and As content reaches up to 0.40 *apfu*. **Pearceite** is an As-dominant member, where Cu content is in a range of 1.53 - 2.48 *apfu*. As is substituted by Sb and its content reaches up to 0.55 *apfu* (Tab. 6, 7).

Minerals of the **tetrahedrite group** were found only rarely as irregular grains and aggregates up to 200 μm size. The grains are homogeneous in BSE images. There are usually accompanied by acanthite (Fig. 6b) and polybasite (Fig. 8b). Two members of tetrahedrite group (Biagioni et al. 2020) were identified in this study: **rozhdestvenskayaite-(Zn)** from the rozhdestvenskayaite subgroup and **argentotetrahedrite-(Zn)** from the argentotetrahedrite subgroup (Sejkora et al. 2021). Rozhdestvenskayaite-(Zn) was found in the sample from the Finsterost vein. Rozhdestvenskayaite-(Zn) is chemically exclusively Ag rich tetrahedrite

with only traces of Cu (maximum 0.03 *apfu*). Ag content ranges between 10.03 and 10.55 *apfu*. The divalent position is dominantly occupied by Zn (1.00-1.58 *apfu*), with elevated Fe content reaching up to 0.93 *apfu*. Traces of Mn were identified up to 0.04 *apfu*. The main constituent in the trivalent trigonal position is Sb substituted by As with Sb/(Sb + As) ratio ranging from 0.83 to 0.93. Sulphur content in the anionic position with octahedral coordination is very variable (Tab. 8), probably due to the presence of vacancies in the crystal structure. Ag content in argentotetrahedrite-(Zn) is in a range of 3.08 - 3.18 *apfu*. Zn is a dominant divalent cation, and its content reaches up to 2.09 *apfu*. The maximum Fe content is 0.31 *apfu*. Trivalent Sb is dominantly substituted by As. Sb/(Sb + As) ratio ranges from 0.83 to 0.94. Relations between dominant cations in tetrahedrites are shown in Figure 11.

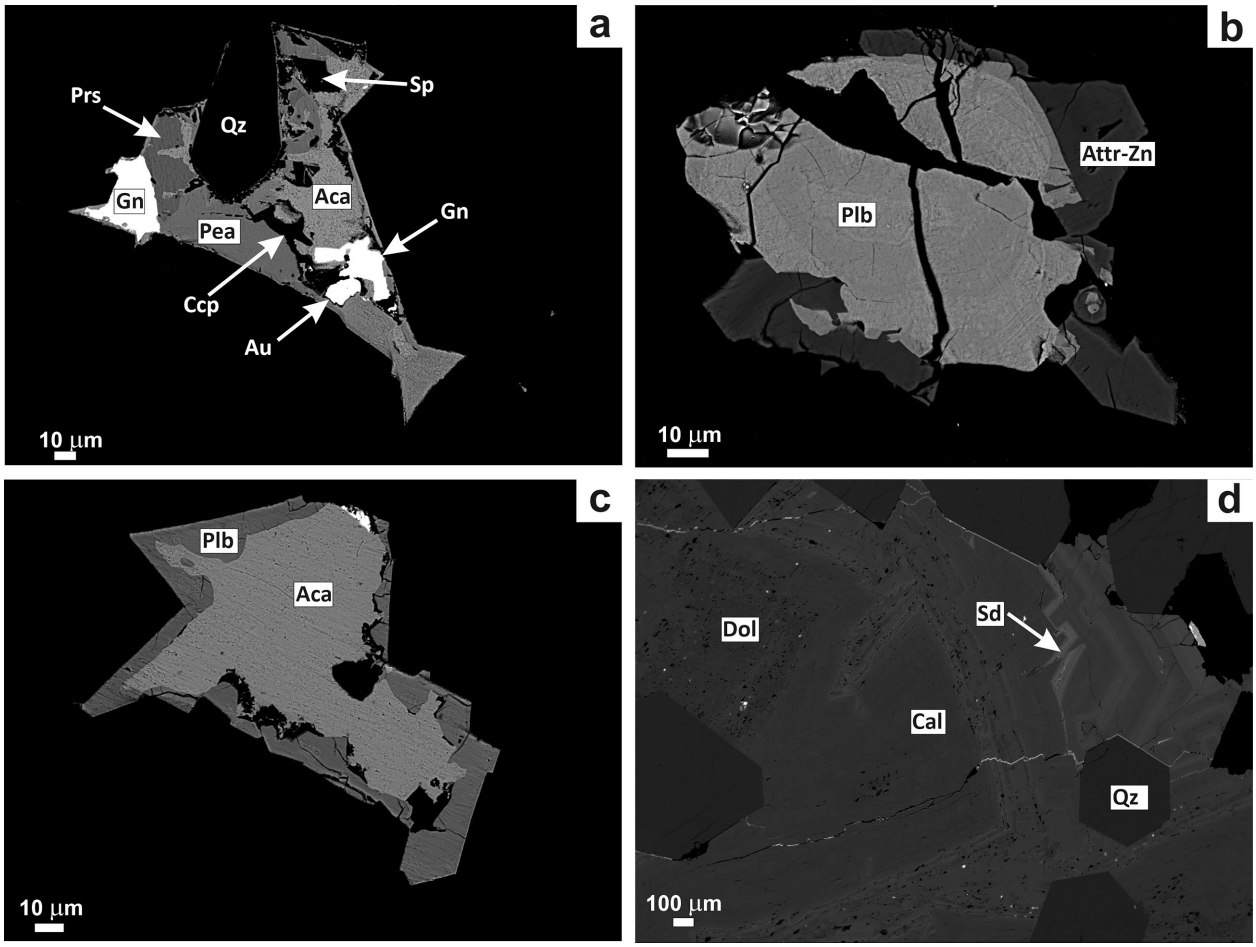

Fig. 8*a* *- Aggregate of silver minerals consisting of acanthite (Aca), proustite (Prs) and pearceite (Pea). They are accompanied by base-metal sulphides: galena (Gn), sphalerite (Sp) and chalcopyrite (Ccp).* ***b*** *- Zoned polybasite (Plb) grain is replacing argentotetrahedrite-(Zn) (Attr-Zn).* ***c*** *- Polybasite (Plb) crystal replaced by acanthite (Aca).* ***d*** *- Intensively zoned aggregates of carbonates (calcite - Cal, dolomite - Dol and siderite - Sd) associated with quartz (Qz). All samples are from the Anton vein. All images are back-scattered images from microprobe.*

Table 3 *Chemical composition of acanthite from the Finsterort (F) and Anton (A) vein*

	F-1	F-2	F-3	F-4	F-5	F-6	A-1	A-2	A-3	A-4	A-5
Ag	87.67	86.12	86.98	84.28	85.03	84.81	86.44	86.43	84.53	84.96	84.13
Te	0.08	0.97	0.11	0.12	0.11	0.11	0.97	0.11	1.00	0.10	0.95
Se	0.00	0.00	0.05	0.00	0.14	0.28	0.00	0.00	0.00	0.00	0.00
As	0.00	0.00	0.00	0.12	0.26	0.07	0.00	0.00	0.00	0.00	0.00
Cu	0.00	0.04	0.10	0.58	0.15	0.13	0.17	0.35	0.15	0.43	0.18
S	11.78	12.40	12.02	13.72	13.21	14.30	12.75	12.76	12.91	13.05	12.53
∑(wt%)	99.53	99.52	99.26	98.81	98.89	99.69	100.33	99.65	98.59	98.54	97.80
Ag	2.065	2.007	2.042	1.920	1.957	1.903	1.988	1.994	1.965	1.965	1.981
Te	0.002	0.019	0.002	0.002	0.002	0.002	0.019	0.002	0.020	0.002	0.019
Se	0.000	0.000	0.001	0.000	0.004	0.008	0.000	0.000	0.000	0.000	0.000
As	0.000	0.000	0.000	0.004	0.009	0.002	0.000	0.000	0.000	0.000	0.000
Cu	0.000	0.002	0.004	0.022	0.006	0.005	0.007	0.014	0.006	0.017	0.007
S	0.933	0.972	0.950	1.051	1.022	1.080	0.987	0.991	1.010	1.016	0.993

Analyses are recalculated on the basis of 3 *apfu*

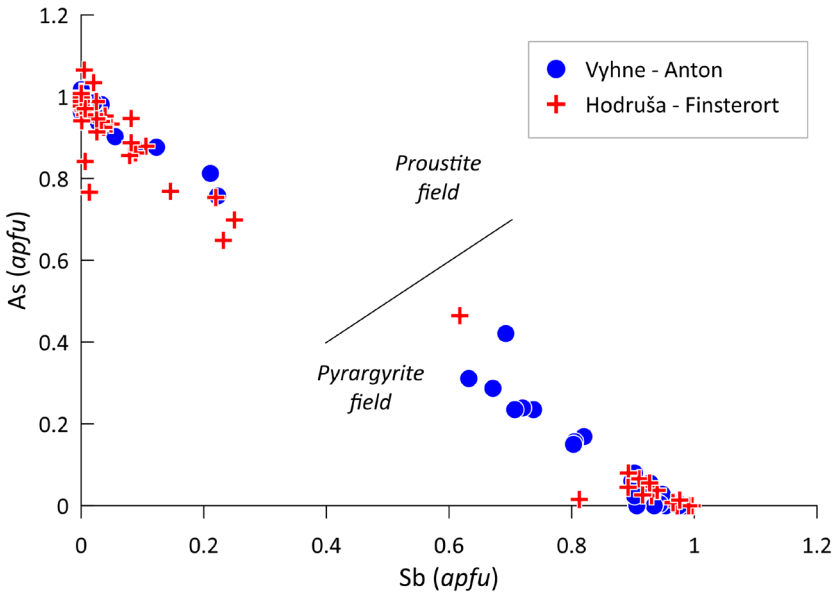

Fig. 9 *Graph of Sb vs. As (apfu) for minerals of the pyrargyrite-proustite solid solution series from the studied localities.*

Table 4 *Chemical composition of pyrargyrite from the Finsterort (F) and Anton (A) vein*

	F-1	F-2	F-3	F-4	F-5	F-6	F-7	A-1	A-2	A-3	A-4	A-5	A-6	A-7
Sb	22.45	22.38	21.26	20.35	20.17	18.35	15.06	22.26	22.18	20.43	16.83	16.58	16.26	15.43
Ag	60.44	61.71	60.97	60.79	60.43	63.95	60.94	60.06	60.44	60.45	60.65	61.17	61.81	61.70
As	0.00	0.00	0.67	1.12	0.62	0.21	6.97	0.00	0.06	1.12	5.30	3.38	3.33	4.06
Pb	0.05	0.04	0.00	0.05	0.05	0.04	0.03	0.07	0.07	0.05	0.06	0.04	0.00	0.10
Cu	0.10	0.03	0.00	0.14	0.18	0.05	0.11	0.26	0.06	0.24	0.17	0.07	0.26	0.14
Fe	0.01	0.56	0.42	0.01	0.00	0.54	0.00	0.00	0.00	0.00	0.00	0.00	0.00	0.00
S	17.60	17.86	18.05	18.04	18.04	17.35	19.83	17.87	18.07	17.80	19.54	18.42	18.18	18.15
∑(wt%)	100.65	102.59	101.36	100.50	99.50	100.49	102.94	100.52	100.89	100.09	102.54	99.66	99.85	99.58
Sb	0.996	0.972	0.927	0.893	0.892	0.813	0.617	0.983	0.975	0.902	0.699	0.720	0.707	0.671
Ag	3.027	3.025	2.999	3.009	3.017	3.197	2.821	2.994	2.998	3.013	2.845	2.998	3.034	3.030
As	0.000	0.000	0.047	0.080	0.045	0.015	0.465	0.000	0.004	0.080	0.358	0.239	0.235	0.287
Pb	0.001	0.001	0.000	0.001	0.001	0.001	0.001	0.002	0.002	0.001	0.001	0.001	0.000	0.003
Cu	0.008	0.002	0.000	0.012	0.015	0.004	0.008	0.022	0.005	0.020	0.014	0.006	0.022	0.011
Fe	0.001	0.053	0.040	0.001	0.000	0.052	0.000	0.000	0.000	0.000	0.000	0.000	0.000	0.000
S	2.966	2.945	2.987	3.005	3.030	2.918	3.088	2.998	3.016	2.984	3.083	3.037	3.002	2.998

Analyses are recalculated on the basis of 7 *apfu*

Table 5 *Chemical composition of proustite from the Finsterort (F) and Anton (A) vein*

	F-1	F-2	F-3	F-4	F-5	A-1	A-2	A-3	A-4	A-5
Sb	6.02	6.56	0.97	0.02	0.00	5.51	3.05	5.13	0.02	0.01
Ag	63.42	64.18	65.14	65.11	65.42	62.29	64.55	64.89	65.18	65.13
Te	0.01	0.03	0.64	0.12	0.07	0.00	0.22	0.05	0.08	0.73
As	10.35	10.96	14.56	15.20	15.00	11.55	13.36	12.17	15.27	15.10
Pb	0.04	0.05	0.05	0.01	0.04	0.13	0.06	0.09	0.15	0.14
Cu	0.22	0.76	0.59	0.56	0.54	0.61	0.29	0.06	0.09	0.16
Fe	0.00	0.02	0.13	0.14	0.03	0.00	0.00	0.00	0.00	0.00
S	19.38	19.12	19.41	19.37	19.60	19.44	19.74	18.97	19.78	19.81
∑(wt%)	99.47	101.68	101.49	100.53	100.70	99.52	101.26	101.36	100.58	101.08
Sb	0.250	0.269	0.039	0.001	0.000	0.227	0.123	0.211	0.001	0.000
Ag	2.973	2.966	2.959	2.969	2.973	2.901	2.941	3.009	2.962	2.951
Te	0.000	0.001	0.025	0.004	0.003	0.000	0.008	0.002	0.003	0.028
As	0.699	0.729	0.952	0.998	0.982	0.774	0.876	0.813	0.999	0.985
Pb	0.001	0.001	0.001	0.000	0.001	0.003	0.001	0.002	0.004	0.003
Cu	0.017	0.060	0.045	0.044	0.042	0.048	0.023	0.005	0.007	0.012
Fe	0.000	0.002	0.011	0.012	0.003	0.000	0.000	0.000	0.000	0.000
S	3.057	2.973	2.967	2.972	2.997	3.046	3.027	2.959	3.024	3.021

Analyses are recalculated on the basis of 7 *apfu*

Gangue minerals

Beside quartz, carbonates are the main gangue minerals of ore vein filling. Carbonates often form euhedral crystals several mm in size. Quartz vugs are usually filled by carbonates. Carbonates show strong oscillatory zoning in BSE images (Fig. 8d). Based on their chemical composition, several carbonates can be recognized (Tab. 9). The chemical composition of carbonates corresponds to **calcite**, **dolomite** and **siderite** (Fig. 12). Calcite and dolomite represent the older carbonate phases. Siderite seems to be younger than calcite and dolomite. Siderite grains are often partly corroded and replaced by Fe-oxy-hydroxides. Silver bearing minerals are hosted in both quartz and calcite / dolomite.

Discussion

The studied localities have very similar mineralogy because they belong to the same epithermal vein system evolved contemporaneously with the same structural pattern. The oldest observed deformation is characterised by low-angle normal faults that are related to exhumation of the Upper Badenian granodiorite intrusion and they are significantly older than the Finsterort and Anton vein system.

The geometry of analysed vein system can be characterised by NNE - SSW strike of vein walls with moderate to steep inclination eastwards. At some places, the vein system is overturned and the dip of partial veins is westwards. Such helicoidal geometry of an individual Riedel shear along the main structure is linked with older strike-slip faulting (cf. Naylor et al. 1986). Moreover, the NNE - SSW strike-slip faults disrupted the oldest low-angle normal faults. Unfortunately, the older strike-slip slickenside lineations are rare because they were overprinted by very intensive later normal faulting. The evolution of the mineralisation process is linked to this extensional tectonic phase. Based on the kinematic analysis, the normal faulting is divided into two stages with different orientation of slickensided lineations on the vein walls. The older transport lineations on fault/vein planes have SE and the younger ENE directions, and these vectors of lineation are distinctive for each part of the vein system.

Based on our mineralogical and paragenetic study, three parageneses of ore minerals can be distinguished, which is roughly in agreement with previous studies (e.g., Koděra 1960, 1969; Berkh et al. 2014). The first paragenesis is dominantly formed by pyrite and base-metal sulphides as galena, sphalerite and chalcopyrite. The second paragenesis is represented by Au-Ag minerals. The crystallization sequence can be proposed as follows: argentotetrahedrite-(Zn) → rozhdestvenskayaite-(Zn) → Au-Ag alloys → pearceite/polybasite → pyrargyrite/proustite → acanthite. The third paragenesis represents uytenbogaardtite and porous acanthite, and it is distinguished by its textural features. This paragenesis is developed on the pre-existing base-metal and precious-metal minerals and could originate in the cementation zone. From the mineralogical perspective, the most interesting is the second mineral paragenesis (Au-Ag bearing). Tetrahedrite group minerals represents the boundary between first and second paragenesis. They are younger than base-metal sulphides, but older than Ag-sulphosalts/sulphides. Rozhdestvenskayaite-(Zn) is a rare member of the tetrahedrite group with monovalent site fully occupied by Ag and was firstly described from the Moctezuma mine, Moctezuma, Sonora, Mexico (Welch et al. 2018). Remarkable geochemical feature of the second ore paragenesis at the Finsterort and Anton veins is the dominant presence of As. The significant amount of As is accommodated in pearceite-polybasite and proustite-pyrargyrite series where As members are dominant. A part of As is present in rozhdestvenskayaite-(Zn) and argentotetrahedrite-(Zn), too. This As enrichment is in contrast with the results from the

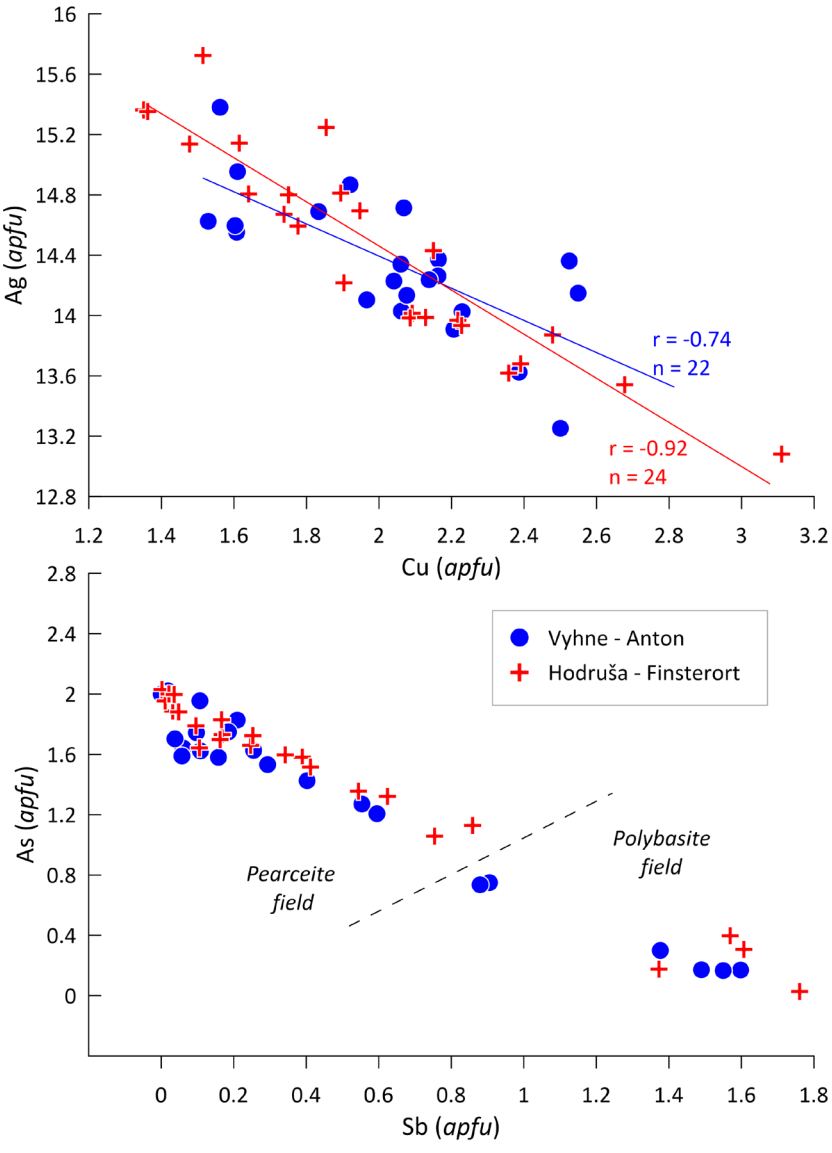

Fig. 10 *Graph of Cu vs. Ag and Sb vs. As (apfu) for minerals of the polybasite-pearceite solid solution series from the studied localities.*

Rabenstein occurrence near Hodruša - Hámre, where all ore minerals are unusually As-poor (Majzlan 2009; Berkh et al. 2014). As zonation is well documented in pyrargyrite-proustite series and indicates variations in the composition of the ore-forming fluids (Fig. 6c). The composition of fluids was very variable over a short period of time. Similar complete pyrargyrite-proustite solid solution was described from Kremnica Au-Ag deposit by Števko et al. (2018). Almost complete miscibility between pyrargyrite and proustite observed in studied samples indicates temperatures above 200 - 300 °C (Toulmin 1963; Ghosal et al. 1995). Another noteworthy feature of the studied mineralization is the chemical variability of the carbonates, where calcite, dolomite and siderite were identified. Rapid changes in fluid composition are evident from the strong oscillatory zonation. The strong variability of carbonates associated with the ore minerals was also observed at the Schöpfer vein (Majzlan et al. 2016). The authors suggest that the presence of siderite indicates that the capacity to precipitate sulphides was exhausted most probably by depletion in reduced sulphur, rather than by depletion of metals in the fluid.

Uytenbogaardtite was previously described from the ore mineralizations of the Štiavnica - Hodruša ore field (Majzlan 2009; Berkh et al. 2014; Chovan et al. 2019) and has also been mentioned from the Kremnica ore field (Števko et al. 2018) or from the Nová Baňa ore field (Majzlan et al. 2018), too. Generally, uytenbogaardtite occurs in association with electrum and/or acanthite, and its deposition is either late hydrothermal (low-temperature) or has been formed in the supergene stage (alteration stage). Thermodynamic modelling supports the idea that this mineral can originate at low temperatures (as low as 25 °C), even if the fluids are relatively oxidizing (Palyanova, Savva 2008).

The origin of paragenetically similar low-sulphidation precious metal mineralizations occurring at the Hodruša - Hámre, Nová Baňa and Kremnica was studied by Koděra et al. (2005, 2014), Majzlan et al. (2016, 2018) and Kubač et al. (2018) based on fluid inclusion and stable isotope studies. According to these authors, the source of fluids is a mixture of meteoric and magmatic water. Fluid inclusions show low salinities of aqueous fluids (0.5 to 5 wt. % NaCl eq.), but locally could be increased up to the 24 wt. % NaCl

Table 6 *Chemical composition of polybasite from the Finsterort (F) and Anton (A) vein*

	F-1	F-2	F-3	F-4	A-1	A-2	A-3	A-4
Sb	8.94	8.59	8.38	7.60	8.66	8.50	7.96	7.57
Ag	70.78	72.73	72.71	66.36	69.02	69.16	72.83	70.91
Te	0.00	0.00	0.00	0.39	0.35	0.00	0.04	0.43
As	0.09	1.01	1.31	0.60	0.57	0.56	0.57	1.01
Pb	0.92	0.03	0.00	0.04	0.05	0.07	0.04	0.02
Cu	4.02	3.80	3.77	7.73	6.12	5.85	4.36	4.62
S	13.13	14.59	14.51	16.23	15.17	15.90	14.62	16.06
∑(wt%)	97.88	100.75	100.68	98.94	99.93	100.04	100.41	100.61
Sb	1.764	1.607	1.569	1.374	1.598	1.550	1.490	1.376
Ag	15.752	15.354	15.365	13.550	14.373	14.229	15.381	14.552
Te	0.000	0.000	0.000	0.067	0.062	0.000	0.006	0.074
As	0.028	0.307	0.398	0.176	0.170	0.166	0.173	0.300
Pb	0.107	0.003	0.000	0.004	0.005	0.008	0.005	0.002
Cu	1.517	1.363	1.352	2.679	2.164	2.041	1.561	1.608
S	9.833	10.366	10.316	11.149	10.628	11.006	10.384	11.088

Analyses are recalculated on the basis of 29 *apfu*

Table 7 *Chemical composition of pearceite from the Finsterort (F) and Anton (A) vein*

	F-1	F-2	F-3	F-4	F-5	F-6	A-1	A-2	A-3	A-4	A-5	A-6
Sb	3.06	2.34	2.18	0.12	0.07	0.01	3.14	2.31	1.63	0.21	0.11	0.00
Ag	69.93	69.78	71.69	73.85	70.15	70.48	69.99	69.17	69.11	72.97	73.33	72.36
Te	0.04	0.61	0.74	0.07	0.80	0.09	0.64	0.70	0.73	0.10	0.10	0.09
As	4.70	5.30	5.45	6.93	6.80	7.13	4.44	5.02	5.24	5.87	7.04	6.88
Pb	0.03	0.03	0.06	0.09	0.04	0.00	0.08	0.04	0.03	0.01	0.07	0.10
Cu	6.15	7.35	6.29	4.82	6.29	6.64	6.54	7.14	6.47	6.04	4.52	4.68
S	16.29	15.79	15.07	15.58	16.07	16.17	16.37	16.66	15.81	15.41	16.07	15.87
∑(wt%)	100.19	101.18	101.48	101.45	100.21	100.53	101.21	101.03	99.02	100.62	101.23	99.99
Sb	0.544	0.412	0.391	0.021	0.011	0.002	0.553	0.402	0.293	0.038	0.019	0.000
Ag	14.015	13.898	14.488	14.809	13.987	13.950	13.908	13.624	14.026	14.714	14.624	14.597
Te	0.007	0.103	0.126	0.012	0.135	0.016	0.108	0.116	0.125	0.017	0.017	0.015
As	1.356	1.518	1.586	1.999	1.953	2.033	1.271	1.425	1.532	1.703	2.021	1.999
Pb	0.003	0.003	0.007	0.009	0.004	0.000	0.008	0.004	0.003	0.001	0.007	0.011
Cu	2.091	2.484	2.158	1.641	2.128	2.230	2.206	2.386	2.229	2.068	1.529	1.604
S	10.985	10.582	10.245	10.508	10.780	10.769	10.945	11.042	10.793	10.458	10.782	10.775

Analyses are recalculated on the basis of 29 *apfu*

eq. due to the boiling of fluids. The ore mineralization was deposited mostly at temperatures between ca. 190 - 270 °C, but locally even at lower temperatures (~160 °C).

Conclusions

The mineralization at the Finsterort - Anton vein system is hosted in the NNE - SSW striking approximately 6 km long vein system in the central zone of the Štiavnica Stratovolcano. The vein fill is related to normal faulting in the Late Miocene. Three parageneses of ore minerals can be distinguished: base-metal paragenesis, precious metal paragenesis and secondary enrichment. Precious metal minerals are represented by rare rozhdestvenskayaite-(Zn), argentotetrahedrite-(Zn), Au-Ag alloys, members of pearceite-polybasite and pyrargyrite-proustite solid solutions, acanthite and uytenbogaardtite. Ore minerals are accompanied by quartz and carbonates (calcite, siderite and dolomite) which are the main gangue.

Table 8 *Chemical composition of the tetrahedrite-group minerals from the Finsterort (F) and Anton (A) vein*

	F-1	F-2	F-3	F-4	F-5	F-6	F-7	A-1	A-2	A-3	A-4	A-5
Sb	18.35	17.01	18.97	19.55	19.90	19.81	19.47	25.64	24.89	22.46	23.01	22.79
Ag	54.09	54.37	53.06	52.36	52.52	52.66	52.99	18.93	18.84	19.34	18.99	18.30
Hg	0.26	0.10	0.34	0.22	0.27	0.21	0.35	0.07	0.00	0.30	0.00	0.00
As	1.74	2.16	2.24	2.14	0.97	1.71	1.70	1.08	1.63	2.73	2.48	2.91
Cu	0.03	0.01	0.01	0.06	0.03	0.08	0.06	25.00	25.08	24.82	25.00	25.48
Fe	1.43	1.68	2.52	2.39	1.10	1.89	2.02	0.22	0.40	0.99	0.29	0.17
Mn	0.05	0.01	0.03	0.02	0.09	0.07	0.03	0.03	0.02	0.00	0.04	0.02
Pb	0.01	0.05	0.06	0.00	0.03	0.07	0.07	0.00	0.04	0.23	0.21	0.03
S	19.25	19.36	19.77	20.14	19.38	19.50	19.85	23.55	23.16	23.58	23.19	23.67
Zn	4.33	3.97	3.16	3.37	4.91	4.27	4.58	7.00	6.84	6.05	5.98	7.86
∑(wt%)	99.52	98.73	100.16	100.24	99.20	100.28	101.12	101.51	100.89	100.50	99.21	101.24
Sb	3.133	2.924	3.222	3.331	3.433	3.351	3.265	3.721	3.603	3.266	3.398	3.254
Ag	10.423	10.549	10.173	10.071	10.229	10.053	10.029	3.100	3.079	3.175	3.165	2.950
Hg	0.027	0.011	0.035	0.023	0.028	0.022	0.036	0.006	0.000	0.027	0.000	0.000
As	0.482	0.604	0.618	0.593	0.272	0.471	0.464	0.254	0.383	0.644	0.596	0.676
Cu	0.009	0.004	0.002	0.019	0.009	0.027	0.019	6.950	6.954	6.916	7.072	6.970
Fe	0.531	0.628	0.934	0.886	0.412	0.698	0.740	0.069	0.127	0.313	0.093	0.054
Mn	0.020	0.005	0.011	0.007	0.036	0.025	0.011	0.009	0.007	0.000	0.012	0.006
Pb	0.001	0.005	0.006	0.000	0.003	0.007	0.007	0.000	0.003	0.020	0.018	0.002
S	12.478	12.640	12.750	13.032	12.699	12.529	12.637	12.976	12.734	13.024	13.004	12.836
Zn	1.375	1.270	0.999	1.070	1.579	1.346	1.429	1.892	1.844	1.639	1.645	2.089

Analyses are recalculated on the basis of 16 cations

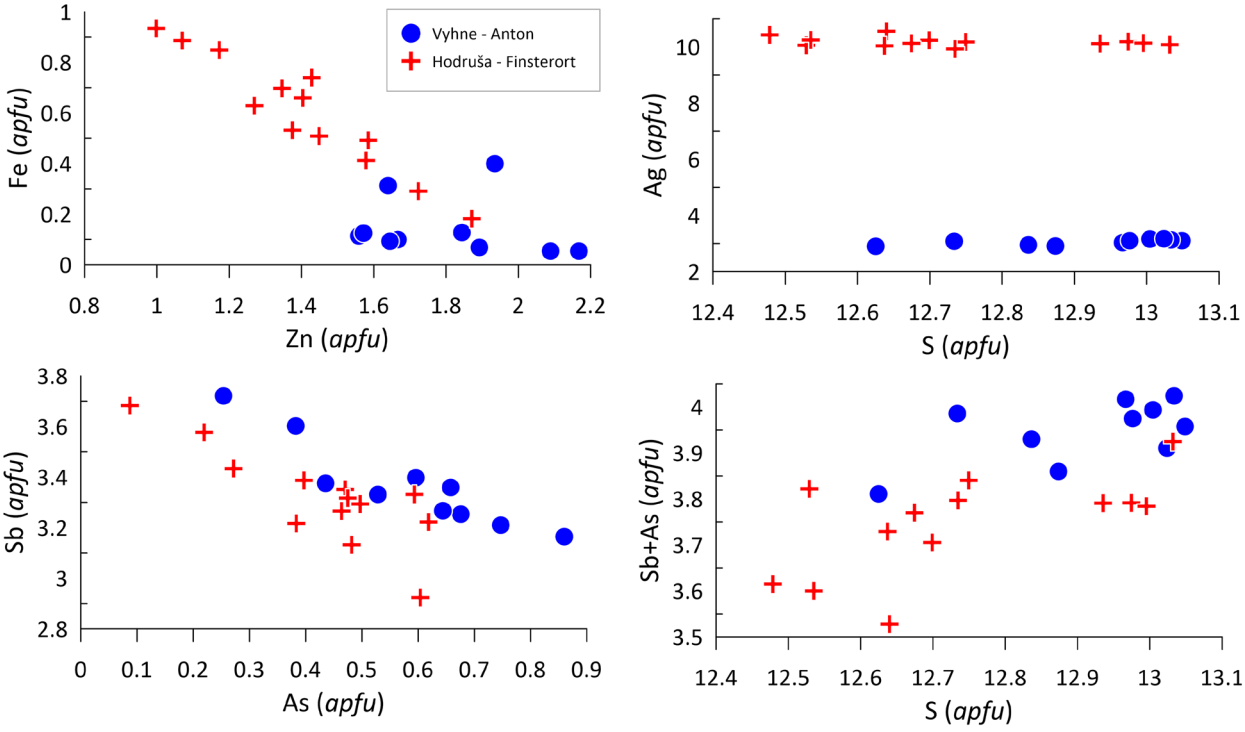

Fig. 11 *Substitution trends for members of the tetrahedrite group from the Finsterort and Anton vein.*

Table 9 *Chemical composition of carbonates from the Finsterort (F) and Anton (A) vein*

	F-1	F-2	F-3	F-4	F-5	F-6	F-7	A-1	A-2	A-3	A-4	A-5	A-6	A-7
MgO	1.94	2.56	2.28	3.93	1.72	4.34	3.85	17.72	17.35	14.91	4.16	4.29	3.45	2.76
FeO	0.36	0.04	0.07	47.34	50.79	48.01	46.55	1.68	4.14	6.52	46.88	46.83	46.73	47.87
MnO	0.17	0.24	0.04	3.58	2.47	3.21	3.82	0.25	0.63	0.41	3.47	3.11	3.43	4.29
CaO	54.05	54.46	53.76	5.81	2.30	5.48	6.15	32.94	30.93	32.23	5.74	5.74	6.03	5.43
SrO	0.00	0.00	0.02	0.00	0.00	0.06	0.02	0.00	0.09	0.00	0.00	0.02	0.02	0.01
CO_2	45.18	44.72	45.35	40.14	43.87	40.51	40.03	45.73	45.52	44.83	40.08	39.94	39.39	39.51
∑(wt%)	101.69	102.01	101.53	100.79	101.16	101.61	100.42	98.32	98.66	98.91	100.32	99.93	99.05	99.86
Mg	0.047	0.061	0.056	0.107	0.052	0.117	0.105	0.417	0.410	0.355	0.114	0.118	0.096	0.077
Fe	0.005	0.001	0.001	0.724	0.856	0.727	0.714	0.022	0.055	0.087	0.719	0.720	0.729	0.747
Mn	0.002	0.003	0.001	0.055	0.042	0.049	0.059	0.003	0.009	0.006	0.054	0.048	0.054	0.068
Ca	0.946	0.935	0.943	0.114	0.050	0.106	0.121	0.557	0.526	0.552	0.113	0.113	0.121	0.109
Sr	0.000	0.000	0.000	0.000	0.000	0.001	0.000	0.000	0.001	0.000	0.000	0.000	0.000	0.000
Analyses are recalculated on the basis of 1 cation														

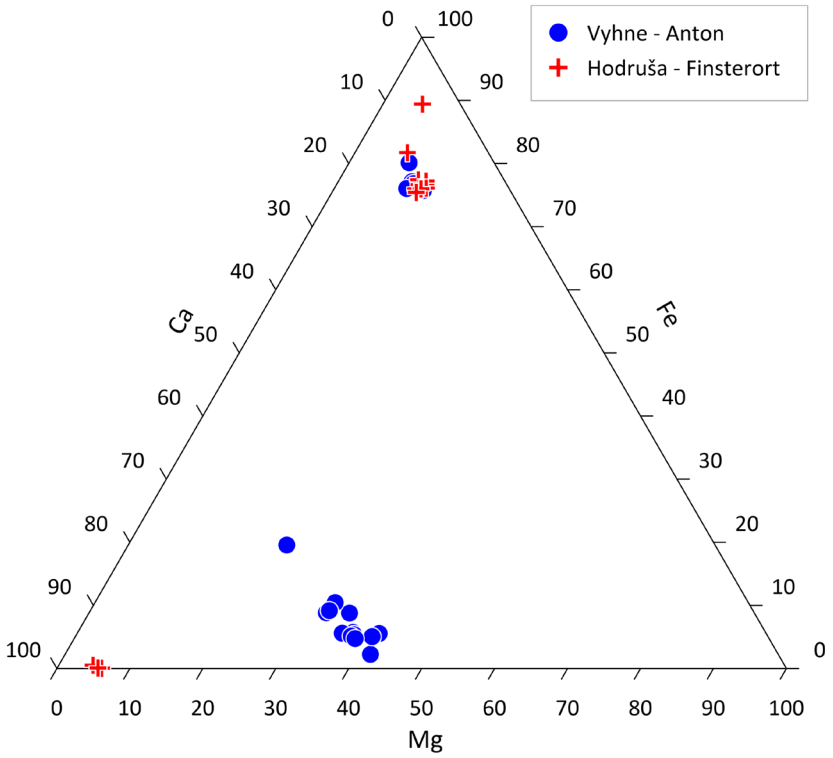

Fig. 12 *Ternary Ca-Mg-Fe plot for carbonates from the Finsterort and Anton vein.*

Acknowledgements

This work was financially supported by the VEGA projects (2/0028/20 and 1/0346/20). We are thankful to the handling editor J. Sejkora and reviewers M. Števko and L. Vrtiška for constructive critical comments which helped to improve the manuscript.

References

Angelier J (1990) Inversion of field data in fault tectonics to obtain the regional stress - III. A new rapid direct inversion method by analytical means. Geophys J Int 103: 363-376

Angelier J (1994) Fault slip analysis and paleostress reconstruction. In: Hancock PL (Ed.) Continental deformation. Pergamon Press, University of Bristol (U.K.), London: 53-100

Bakos F, Chovan M, Žitňan P (Ed.) (2017) Gold in Slovakia. Lúč, Bratislava, 1-429

Berkh K, Majzlan J, Chovan M, Kozák J, Bakos F (2014) Mineralogy of the Medieval Ag-Au occurrences Banská Belá, Treiboltz, Rabenstein, and Kopanice in the Banská Štiavnica ore district (Slovakia). N Jb Miner, Abh 191(3): 237-256

Biagioni C, George LL, Cook NJ, Makovicky E, Moëlo Y, Pasero M, Sejkora J, Stanley ChJ, Welch MD, Bosi F (2020) The tetrahedrite group: Nomenclature and classification. Am Mineral 105: 109-122

Ďuďa R, Ozdín D (2012): Minerály Slovenska. Granit, Praha, 1-480

Ghosal S, Sack RO (1995) As-Sb energetics in argentian sulfosalts. Geochim Cosmochim Acta 59: 3573-3579

Chovan M, Kubač A, Mikuš T, Žitňan P, Prcúch J (2019) Au-Ag tellurides and sulphosalts from epithermal Au -Ag-Pb-Zn-Cu deposit Banská Hodruša at the Rozália mine (Slovakia). Acta Geol Slov 11(2): 43-62

Etchecopar A, Vasseur G, Daignieres M (1981) An inverse problem in microtectonics for the determination of stress tensor from fault striation analysis. J Struct Geol 3: 51-65

Kaňa R (2016) Odkazy minulosti. Banskoštiavnicko-hodrušský banícky spolok, Banská Štiavnica, 1-190

Koděra M (1960) Paragenetic and geochemical research of the Všechsvätých vein in Hodruša. Acta Geol Geogr Univ Comen 4: 69-105 (in Slovak)

Koděra M (1963) Gesetzmässigkeiten der zonalen Verteilung der Mineralisation an der subvulkanischen polymetallischen Lagerstätte Banská Štiavnica. In: Problems of Postmagmatic Ore Deposition 1. Geological Survey of Czechoslovakia, Prague, Czech Republic: 184-189

Koděra M (1969) To the question about the relationship between the Banská Štiavnica and the Hodruša ore fields. Mineral Slov 3-4: 247-250

Koděra M (ed.) (1986) Topographic Mineralogy of Slovakia. Veda, the Publishing House of Slovak Academy of Sciences, 462-472 (in Slovak)

Koděra P, Lexa J, Rankin AH, Fallick AE (2005) Epithermal gold veins in a caldera setting: Banská Hodruša, Slovakia. Mineral Depos 39: 921-943

Koděra P, Lexa J, Fallick AE, Wälle M, Biroň A (2014) Hydrothermal fluids in epithermal and porphyry Au depositsin the Central Slovakia Volcanic Field. Geol Soc Lond Spec Publ, 402: 177-206

Konečný V, Lexa J, Hojstričová V (1995) The Central Slovakian volcanic field: a review. Acta Volcanol 7: 63-78

Konečný V, Lexa J, Halouzka R, Dublan L, Šimon L, Stolár M, Nagy A, Polák M, Vozár J, Havrila M, Pristaš J (1998) Geology map of Štiavnické Vrchy Mts. and Pohronský Inovec Mts. (Štiavnica Stratovolcano). Geologická Služba Slovenskej republiky, Bratislava.

Konečný V, Kováč M, Lexa J, Šefara J (2002) Neogene evolution of the Carpatho-Pannonian region: an interplay of subduction and back-arc diapiric uprise in the mantle. EGU Stephan Mueller Special Publication Series 1: 105-123

Kovalenker VA, Naumov VB, Prokofev VY, Jeleň S, Háber M (2006) Compositions of magmatic melts and evolution of mineral-forming fluids in the Banská Štiavnica epithermal Au-Ag-Pb-Zn deposit, Slovakia: A study of inclusions in minerals. Geochem Int 44(2): 118-136

Kubač A, Chovan M, Koděra P, Kyle JR, Žitňan P, Lexa J, Vojtko R (2018) Mineralogy of the epithermal precious and base metal deposit Banská Hodruša at the Rozália Mine (Slovakia). Mineral Petrol 112: 705-731

Lexa J (2001) Metallogeny of the Banská Štiavnica stratovolcano. Mineral Slov 33: 203-214 (in Slovak)

Lexa J, Štohl J, Konečný V (1999a) The Banská Štiavnica ore district: relationship between metallogenetic processes and the geological evolution of a stratovolcano. Mineral Depos 34: 639-654

Lexa J, Koděra P, Prcúch J, Veselý M, Šály J (1999b) Multiple stages of mineralization at the Rozália mine, Hodruša. In Thompson BT (Ed.) Epithermal Mineralization of the Western Carpathians. Soc Econ Geol, Guidebook ser 31: 229-247

Majzlan J (2009) Ore mineralization at the Rabenstein occurrence near Banská Hodruša, Slovakia. Mineral Slov 41: 45-54

Majzlan J, Berkh K, Koděra P, Števko M, Bakos F, Milovský R (2016) A mineralogical, fluid inclusion, and isotopic study of selected epithermal Ag-Au occurrences in the Banská Štiavnica - Hodruša-Hámre ore district, Western Carpathians. Acta Geol Slov 8(2): 133-147

Majzlan J, Berkh K, Kiefer S, Koděra P, Fallick AE, Chovan M, Bakos F, Biroň A, Ferenc Š, Lexa J (2018) Mineralogy, alteration patterns, geochemistry, and fluid properties of the Ag-Au epithermal deposit Nová Baňa, Slovakia. Mineral Petrol 112: 1-23

Michael AJ (1984) Determination of stress from slip data: faults and folds. J Geophys Res 89(13): 11517-11526

Naylor MA, Mandl G, Supesteijn CHK (1986) Fault geometries in basement-induced wrench faulting under different initial stress states. J Struct Geol 8(7): 737-752

Onačila D, Rojkovičová Ľ (1992) Precious metal mineralization on the Hodruša ore field veins. Mineral Slov 24 (3-4): 245-256 (in Slovak)

Palyanova GA, Savva NE (2008) Some sulfides of gold and silver: Composition, mineral assemblage, and conditions of formation. In: Theoretical Foundations of Chemical Engineering 42(5): 749-761

Rottier B, Audétat A, Koděra P, Lexa J (2020) Magmatic evolution of the mineralized Stiavnica volcano (Central Slovakia): Evidence from thermobarometry, melt inclusions, and sulfide inclusions. J Volcanol Geotherm Res 401: 1-23

Sejkora J, Biagioni C, Števko M, Raber T, Roth P (2021) Argentotetrahedrite-(Zn), IMA 2020-069. CNMNC Newsletter 59; Mineral Mag 85: https://doi.org/10.1180/mgm.2021.5

Števko M, Sejkora J, Dolníček Z, Škácha P (2018) Selenium-rich Ag-Au mineralization at the Kremnica Au-Ag epithermal deposit, Slovak Republic. Minerals 8: 572

Turner FJ (1953) Nature and dynamic interpretation of deformation lamellae in calcite of three marbles. Am J Sci 251: 276-298

Toulmin P (1963) Proustite-pyragyrite solid solution. Am Mineral 48: 725-736

Vojtko R, Žitňan P, Prcúch J, Lexa J, Koděra P, Chovan M, Kubač A (2019) Structural control of the Banská Hodruša ore deposit (Štiavnica Stratovolcano). In Broska I, Kohút M, Tomašových A (Ed.) Proceedings of the Geologica Carpathica 70 conference. Smolenice Castle, Slovakia, October 9 - 11, 201, Earth Science Institute of the Slovak Academy of Sciences, Bratislava: 45-48

Warr LN (2021) IMA-CNMNC approved mineral symbols. Mineral Mag 85: 291-320

Welch MD, Stanley CJ, Spratt J, Mills SJ (2018) Rozhdestvenskayaite $Ag_{10}Zn_2Sb_4S_{13}$ and argentotetrahedrite $Ag_6Cu_4(Fe^{2+},Zn)_2Sb_4S_{13}$: two Ag-dominant members of the tetrahedrite group. Eur J Mineral 30: 1163-1172